Fiber Morphology of Spider Silk: The Effects of Tensile Deformation

David T. Grubb* and Lynn W. Jelinski

Department of Materials Science and Engineering, Center for Advanced Technology and Biotechnology, Cornell University, Ithaca, New York 14853

Received August 28, 1996[⊗]

ABSTRACT: The fiber morphology of the dragline silk of *Nephila clavipes* has been investigated by the detailed analysis of wide-angle X-ray diffraction (WAXD) patterns. WAXD gives the crystal lattice dimensions, the orientation distribution, the crystalline fraction, and an estimate of the crystal size. It is found that the crystals are very small and well oriented. The mean (minimum) crystal dimensions are $2 \times 5 \times 7$ nm, and the angle, ϕ, between the molecular chains in the crystals and the fiber axis has a full width at half-maximum (fwhm) of 15.7° and an orientation function $f = 0.981$. The X-ray crystallinity is in the range 10−15%, and the amorphous diffraction is divided 60:40 between an isotropic ring and an oriented halo with fwhm 30°. This means one-third of the material is in the oriented amorphous state, with a chain orientation of fwhm 43° and $f = 0.87$. When the fiber is extended up to 10%, the orientation of the crystals increases as predicted for affine deformation at constant volume. There is no observable change in crystallinity and apparently a small reduction in the lateral crystal size on deformation.

Introduction

Spider silk fibers are of practical interest because of their excellent mechanical properties,[1,2] in particular their toughness and high compressive strength. They are formed in the silk gland from a water-based solution, and processing fibers from such a solution is also of great interest. It is generally accepted that the dragline fibers are composed of two very closely related proteins[3] with molecular weight >300 000,[4] and it may be possible to produce these proteins using the tools of biotechnology.[5] Previous X-ray studies on silks have established the general crystal structure as pseudo-orthorhombic containing β-pleated sheets.[6,7] The unit cell dimensions for the crystalline component of the dragline silk of *Nephila clavipes* have been found to be $a = 1.06$, $b = 0.944$, and $c = 0.695$ nm.[8] Warwicker[7] compared and classified many different silks, and from its amino acid composition and unit cell parameters *N. clavipes* falls in group 3b. Other silks in this group have crystals that contain only alanine,[9] and NMR studies of *N. clavipes* show that this too has crystals of poly(alanine).[10,11] The changes in lattice parameter that occur when the fiber is stretched have been measured for silk from the silkworm, *Bombyx mori*,[12] and from *N. clavipes*.[8] The X-ray results are in general similar to those obtained from a wide range of synthetic semicrystalline polymers, except that the degree of order in the silk fibers is much lower than that in most commercial synthetic fibers.

Spider silk fibers shrink when they are wetted with water,[13,14] and this particular class of material shrinks to about 50% of its original length.[14] The shrinkage indicates that the fiber contains molecules that are frozen into a glassy partially extended state; these molecules retract to a random coil when mobilized with water. In the wet state, thermomechanical tests show that the fiber acts as an elastomer.[15] The rigid crystals act as filler particles in this elastomer, increasing its stiffness. In comparison, many textile fibers have molecular orientation without much molecular extension, so that when the disordered molecules are mobilized by heating the shrinkage is small. However, some high performance synthetic materials such as high modulus polyethylene have high molecular extension and the fibers can shrink to a small fraction of their original length.

Recently NMR has been used to derive a detailed model of the fiber structure.[10] Focusing on the alanine residues only, it is found that 40% are in a crystalline environment, in well-oriented β-sheet crystals of poly(alanine). This corresponds to about 10% of the whole fiber. The rest of the alanines are in a phase of intermediate order, less well-oriented than the crystals and corresponding to very small fragments of hydrogen-bonded sheet. Wetting the fiber did not change the mobility of molecules in either of these alanine domains but made large changes to the rest of the silk, which was presumed to be amorphous.[10] Although a two-phase model is traditional in synthetic semicrystalline polymers, both isotropic material and fibers studied in more detail may be interpreted as having three phases.[16,17] The WAXD patterns from poly(ethylene terephthalate) fibers have been fitted as the sum of an isotropic amorphous ring, a highly oriented array of crystals, and an oriented noncrystalline phase.[17] NMR shows that one part of the materials has a relaxation time that lies between the crystal and the amorphous relaxation time and is distinct from both.[18] This is also the case for the spider silk fibers,[10,11] and it strongly supports the existence of a third phase with specific properties. In this and following discussion, the word "phase" is not meant to imply a phase as an independent and stable state of the material.

Another model that describes specific details of spider silk fiber structure has been derived from transmission electron microscopy.[19,20] Comparatively large objects (>50 nm) were seen in TEM images of sections of fiber, and these were identified with the crystalline phase of the protein, although selected area diffraction from these objects did not match the WAXD pattern spacings. It was explained in the paper[19] that the small poly(alanine) crystals would not be visible in the TEM, but it is difficult to explain why the diffraction spacings seen in the TEM are not seen in X-ray diffraction, as the objects took up 50% of the fiber volume. The WAXD pattern from the fiber has broadened peaks, and the

* Author to whom correspondence should be addressed.
[⊗] Abstract published in *Advance ACS Abstracts,* May 1, 1997.

S0024-9297(96)01293-4 CCC: $14.00

broadening is usually described in terms of the size of an ideal perfect crystal that would diffract in this way. However broadening can be produced by small size or by crystal defects. X-ray diffraction can in principle distinguish between the two effects, but not in practice with the patterns obtained from spider silk fibers. Large crystalline objects such as those seen in the TEM could produce the broad X-ray reflections observed, if a highly disordered lattice is present.

Experimental Section

N. clavipes spiders obtained from Central Florida were silked at 2 cm/s in the usual manner[21] with the dragline silk only selected, and the silk collected as rings of 200−3000 filaments. For diffraction, fiber rings were held in a stretching frame mounted on a rotation stage. The rings were not gripped in clamps, but looped over plated steel hooks. Friction in the large number of turns prevented slippage. Wide-angle X-ray diffraction was obtained at the Cornell High Energy Synchrotron Source (CHESS), beam line F1, using 0.091 nm radiation. A 0.3 mm diameter point collimator limited the double-focused beam. A helium-filled tube with a beryllium front window took up all but a few cm of the 1670 mm distance from specimen to detector. The detector was a Fuji imaging plate detector system, giving a 14 bit digital image with 2000 × 2500 pixels, each 0.1 mm square. With this detector and a specimen of cross-sectional area of about 0.04 mm^2 a good fiber pattern could be obtained with a 10 second exposure. The data extend to a scattering vector $s = (\sin\theta)/\lambda$ of 3−4 nm^{-1}, but strong diffraction from the beryllium window and shadowing by the tube made it difficult to use all of the data.

The data were analyzed using a combination of commercially available software. Spyglass Transform was used for display, centering and trimming the pattern. The analysis used sequential rather than "whole pattern" fitting. That is, radial and circumferential scans were obtained from the image, using Matlab. The "radial" scans were actually intensity as a function of radius averaged over a small sector, typically 2−3° wide. Radial data obtained with no sample present was subtracted from these data. The form of a monotonically decreasing background was derived from meridional data, and used as a background in fitting all radial scans. The peaks were fitted with various analytical functions using nonlinear least-squares fitting in Genplot. In principle, it would be better to fit the whole pattern by allowing all crystallographic, crystal size, and orientation variables to vary at once. This Reitveld method has been applied to fiber diffraction patterns recorded as images[22] and recorded as multiple diffractometer scans.[23,24,17] However in these cases the fibers were more highly crystalline and the crystals in the fiber were much larger (or more perfect). Here the broader reflections make the exact choice of the shape of the reflection important, and whole pattern fitting has so far been unsuccessful.

Results and Discussion

A representative fiber pattern from dry and taut but unstretched spider silk is shown in Figure 1. The inner, weaker, peak on the equator corresponds to the distance between the hydrogen-bonded β-pleated sheets. Using the unit cell description of Warwicker,[7] this is (200). The second and more prominent equatorial peak could be (210), (120), or a mixture of the two on the basis on lattice spacing. The structure of β-poly(L-alanine) crystals[25] predicts that (210) will not be present. Assuming that the crystals are close to poly(alanine) the second reflection is taken to be (120). [Arnott uses a different unit cell, reversing **a** and **b** and halving **b** so that the planes described here as (120) are (110) in ref 25.] Because the X-ray wavelength was 0.091 nm, the misorientation required to see the (002) peak was only 7.5°, and a clear (002) was visible even when the fiber was close to perpendicular to the X-ray beam.

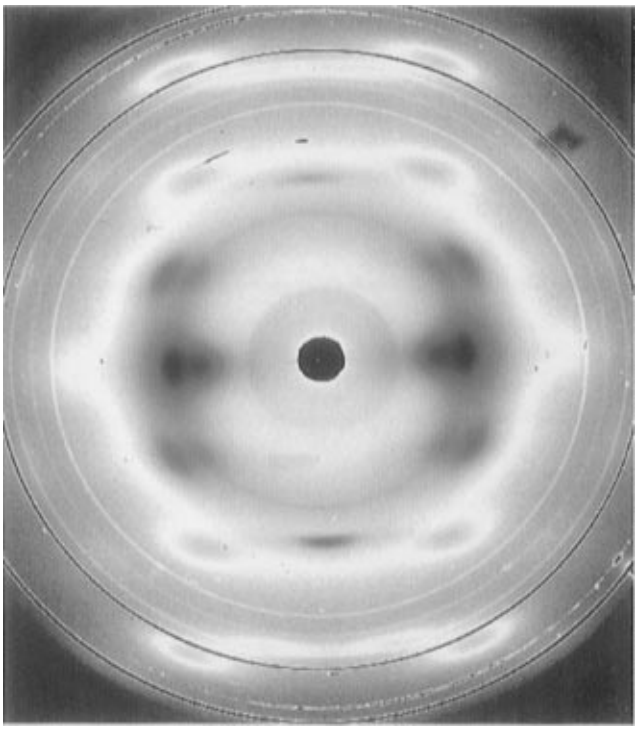

Figure 1. X-ray fiber pattern from a small dry bundle of dragline silk from *N. clavipes*.

Orientation Distribution. The orientation distribution of the structural elements was obtained from circular scans of the intensity. Figure 2a is a plot of the intensity as a function of angle from the equator at the radial position of the strong (120) peak, and Figure 2b is the plot at the position of the (200). The (201) planes have almost the same spacing as the (120), so these first layer line peaks appear as subsidiary peaks in Figure 2a. The overlap makes the fitting more complicated, but ambiguity is removed when the position of the subsidiary peak maximum is fixed at the angle calculated from the unit cell geometry, 37.7°. A single Gaussian curve cannot fit the central peak, but it can be fitted well with either a single Pearson VII function with an exponent of about 1.4, or as two Gaussians, one much wider than the other. The superposed lines on Figure 2a show this two-Gaussian fit. For the dry fibers held at or above their original length, the initial guessed values of the Gaussian widths are not important, as the same final result is always obtained. This was not the case for wet and contracted fibers. Orientation distributions are usually modeled as Gaussian, but there is no reason why other distributions could not exist and apparently no *a priori* reason for choosing one fitting function over the other.

The fitted functions in Figure 2 show that at an angle of 20° to the equator, the intensity is almost completely derived from the broader Gaussian; the subsidiary (201) peaks are too far out and the sharp Gaussian has already died away. (Again, this was not the case for the less well oriented fibers after contraction.) Figure 3 shows superimposed plots of the intensity as a function of q ($=4\pi(\sin\theta)/\lambda$) along the equator and along a line of 20° to the equator. The off-equator intensity is distorted by extra intensity at higher q due to a (hkl) reflection, but it is clear that the intensity is spread into a broad band or halo, while the (200) and (120) crystalline reflections are perfectly clear in the equatorial plot. The halo is so broad that the material that produces it is best described as amorphous. There is crystalline

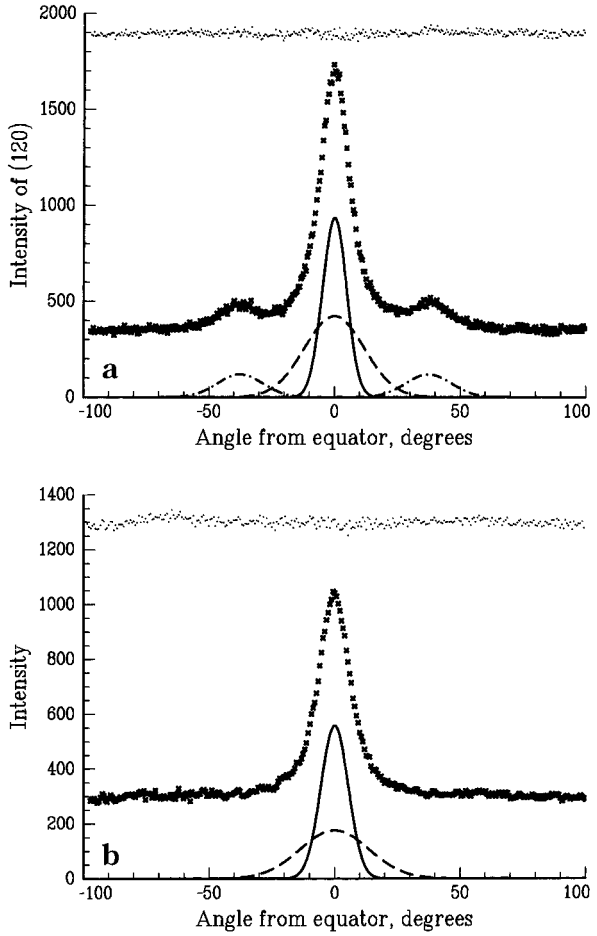

Figure 2. Intensity as a function of angle from the equator: (a) at the radial position of the strong equatorial (120) peak; (b) at the radial position of the weaker inner equatorial (200) peak.

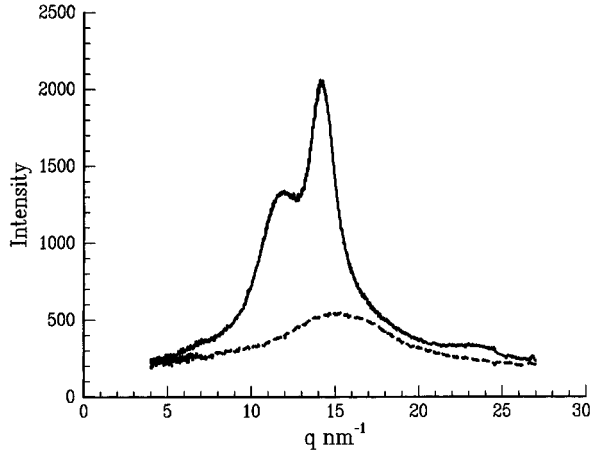

Figure 3. Intensity as a function of scattering vector $q = 4\pi(\sin\theta)/\lambda$. The solid line is the intensity along the equator. The dashed line is the intensity along a line at 20° to the equator. The crystalline reflections are absent at 20° to the equator.

material that is well oriented in addition to less well-oriented amorphous material. This is a sound basis for preferring the two Gaussian fit of the data in Figure 2 and relating each angular distribution to a different component of the material; the single Pearson function includes both the crystalline regions and the partially oriented amorphous material.

Table 1 shows the data for angular distribution for both the Pearson and the two Gaussian fits to the (120) and to the (200) reflection for a dry fiber bundle stretched in tension. The (200) has no subsidiary peaks in the angular intensity plot (Figure 2b), but it is weaker and less accurate. The angles drop with increasing strain, but the changes are quite small, so that it is not surprising that an earlier X-ray study[26] and NMR orientation measurements[10] did not detect any reorientation. The (200) is less well oriented than (120) and the (200) orientation changes more than the (120) orientation. The results are given in terms of a full width at half-maximum for the relevant planes about the equator. We can obtain the orientation of the molecular chains about the fiber axis from this data. For a given orientation, $\sum\cos^2\phi_i = 1$ when the ϕ_i are measured from any orthogonal axis set. For two reflections which are not orthogonal but have a known geometry in the equatorial plane

$$\langle\cos^2\phi_3\rangle = 1 - A\langle\cos^2\phi_1\rangle - B\langle\cos^2\phi_2\rangle \qquad (1)$$

Take axis 1 to be (200), axis 2 to be (120), and axis 3 to be the fiber axis, (002). (120) is 65° from the (200), so $A = 0.8$ and $B = 1.2$. The data in Table 1 are measured from the equator and not the fiber axis, so with $\Psi = (90 - \phi)$ eq 1 becomes

$$\langle\cos^2\phi_3\rangle = 1 - A\langle\sin^2\Psi_1\rangle - B\langle\sin^2\Psi_2\rangle \qquad (2)$$

For a Gaussian, $\langle\cos^2\phi\rangle = \{\cos(0.4\ \text{fwhm})\}^2$ and for a Pearson VII function with exponent 1.4, $\langle\cos^2\phi\rangle = \{\cos(0.55\ \text{fwhm})\}^2$. The data in Table 1 can thus be used to find the orientation of the molecular chains about the fiber axis in terms of a fwhm or as the orientation function $f = (3\langle\cos^2\phi_3\rangle - 1)/2$.

Figure 4 shows the results of this procedure for both fits to the data. For affine deformation at constant volume the tangent to the angle is proportional to $(1 + \text{strain})^{-3/2}$ and this prediction is shown as dashed lines. (In all these plots, the values at 0.06 strain are not good because the total intensity for this measurement was very low due to specimen misalignment.) The circles represent data obtained during the slow stretching. The fibers broke on stretching from 0.10 to 0.12 strain, and data obtained after the break is plotted as the *X* at zero strain, because the bundle was no longer under load. The Pearson VII data in Figure 4a are very close to the affine deformation prediction, and the "crystalline" sharper Gaussian (Figure 4b) is also good, although the errors are greater. From Figure 4b the fwhm of the chain axis in crystals in unstretched fibers is 17°. The oriented amorphous or broad Gaussian peak (Figure 4c) shows a trend of increasing orientation with strain, but the scatter is large. The lower data sets and solid lines in parts a and b of Figure 4 are obtained by correcting for crystal size effects, as described below.

A direct measurement of chain orientation using a meridional (00*l*) is normally thought to require a sample tilted by exactly the Bragg angle. However, if the orientation distribution is Gaussian, measurement of a misaligned fiber will give the same angular width, and exact orientation is not necessary. This is because a radially symmetric Gaussian will give the same fwhm if tested on a straight line that does not pass through the center. If we have $I = \exp(-r^2/w^2)$, then $I = \exp[-(x^2 + y^2)/w^2]$ so, at constant y, $I = C\exp(-r^2/x^2)$. The curvature of the Ewald sphere can be neglected for a well-oriented system.

The (002) reflections tested fit well to a single Gaussian distribution, and the fwhm is 21° in the dry and taut

Table 1. Width of Angular Distribution about the Equator vs Strain for (120) and (200) Reflections from a Dry Fiber Bundle[a]

			two Gaussian functions			
	Pearson VII function		narrow (crystalline)		broad (amorphous)	
strain %	(120)	(200)	(120)	(200)	(120)	(200)
0	13.99 ± 0.003	14.86 ± 0.004	11.24 ± 0.08	12.80 ± 0.01	28.0 ± 0.04	32.33 ± 0.07
2	13.80 ± 0.003	14.47 ± 0.005	11.09 ± 0.06	12.80 ± 0.01	28.2 ± 0.04	35.07 ± 0.07
4	13.49 ± 0.002	13.81 ± 0.004	10.88 ± 0.05	12.07 ± 0.01	28.3 ± 0.05	32.88 ± 0.05
6	12.76 ± 0.008	12.86 ± 0.015	10.21 ± 0.2	10.08 ± 0.06	25.4 ± 0.11	24.7 ± 0.13
8	13.04 ± 0.004	12.91 ± 0.006	10.50 ± 0.08	11.29 ± 0.02	26.9 ± 0.06	28.8 ± 0.08
10	12.72 ± 0.003	12.66 ± 0.006	10.32 ± 0.09	10.95 ± 0.01	27.3 ± 0.05	27.63 ± 0.07
break	13.89 ± 0.01	14.74 ± 0.02	11.20 ± 0.2	11.62 ± 0.08	29.1 ± .2	28.8 ± .022

[a] The reflections are fitted either as a single Pearson VII function or as the sum of two Gaussians. The widths are given as the full width at half-maximum in degrees. The small errors relate only to fitting uncertainty.

state, (0% strain) in good agreement with the results obtained from the equatorial data (Figure 4). However, it is not possible to determine the orientation distribution of the structural elements without some consideration of their size, as indicated by the width of the X-ray reflections. For example, the spread of the (120) reflection away from the equator was considered above to be entirely due to the crystal orientation distribution, but limited size in the **c** direction will spread the spots in much the same way. Similarly, the spread of the (002) is almost parallel to the equator and may be due to a misorientation or the small lateral size of the crystals.

Crystal Size. Radial scans along the equator and along the meridian give the radial peak widths on the (120), (200), and (002) reflections. The shape of the (002) reflection as a function of diffraction angle is clearly asymmetric, with a longer tail at higher angles (Figure 5). This could be caused by overlap with other reflections such as (112) or by the orientational smearing of a sharp reflection. There is a broad amorphous halo and in some cases a sharp peak superimposed on it at close to (but at slightly larger angles than) the position of the strong (120) equatorial peak (Figure 5). This is consistent with the presence of unoriented amorphous material and also in some cases a small amount of well-organized crystalline material that is not oriented. Because it is normally assumed that quantitative results can only come from exactly aligned fibers, the analysis of the meridional peaks was kept simple. The (002) peak fwhm was measured without concern for how the peak came to be asymmetric. The results interpreted as due to a perfect crystal of limited size show a thickness of 5.5−7 nm in the chain direction for all samples, with no correlation to stretching the fiber.

Determining a crystal size in the lateral direction is not straightforward, because the crystalline reflections are broad and overlapped with the strong halo from oriented disordered material. The best fits of the equatorial data were obtained with four Pearson VII functions. The two crystalline peaks are assumed to have the same shape although they are of different widths. The other two peaks are the amorphous peak (oriented + unoriented) and a bump at higher angles that comes from several crystalline reflections. This last peak is included to allow a wide angular range of data to be fitted, but it is not used in further analysis. The equatorial crystalline peaks are so broad that they cannot be unambiguously separated from the underlying amorphous halo. However, consistency requires that the peak height of each crystalline reflection is the same in the angular and in the radial scans. Radial overlap of the peaks means that some intensity from the other peak appears in the angular scan data, so for each equatorial peak we require that radial peak height = sharp Gaussian height from angular fit + overlap from the other peak.

This condition was used to choose a best fit for the radial equatorial data, as shown in Figure 6. Consistency also requires that the broad Gaussian height from the angular fit should be equal to the amorphous halo intensity on the equator minus the amorphous halo intensity on the meridian. This was checked and found to be approximately correct, but was not used in the fitting procedure.

The radial width of the inner (200) peak is much greater than that of the outer. This means that the crystals are thinner or the order poorer perpendicular to the hydrogen-bonded planes, (200), a common observation in silks.[27,28] Assuming a perfect crystal, the reflection width can be simply interpreted as a crystal thickness. The thickness perpendicular to (200) is 2−2.6 nm, and the crystals are wider perpendicular to (120), 3.5−4 nm. This implies a slightly greater width in the hydrogen-bonded plane direction, [010], of 4−5 nm. When the fit described above is used, there is a definite trend to smaller lateral crystal sizes when the crystal is strained. When a constant peak shape is used for the fitting the trend is weaker, but still present. Figure 7 shows the effect for both the (120) and (200) peaks. It is important to realize that these crystal sizes are averages of broad distributions. The (120) and (200) peaks are Pearson VII with exponent 1.7−2.4, close to the modified Lorentzian shape. A uniform distribution of crystal thicknesses from 0 to 2t gives a reflection with exponent 2.4, and for a triangular distribution from 0 to 3t the exponent is 1.6. These are not the only distributions which can give similar curve shapes, but they act as examples to show that there is no expectation that all crystals have a similar size, or that there may not be a continuous distribution of sizes down to the "amorphous" level.

We can now consider the effects of crystal size on the orientation parameters that have been determined, and it is easiest to do this by considering the widths of the reflections in pixels (size 0.1 mm) on the image plane. The angular fwhm of (120) and (200) of 11 and 12° correspond to widths of 60−70 pixels, and the radial width of the (002) corresponds to a reflection width of 22 pixels. The angular width is Gaussian, and the asymmetric Pearson VII used to fit the (002) peaks has a large exponent. Convolution of two such distributions increases their width in quadrature, so that on deconvoluting the effect of crystal size the angular fwhm is reduced from 60−70 to 56−66 pixels, a reduction of 5−7%. This is a comparatively small correction which propagates through the calculation of chain orientation,

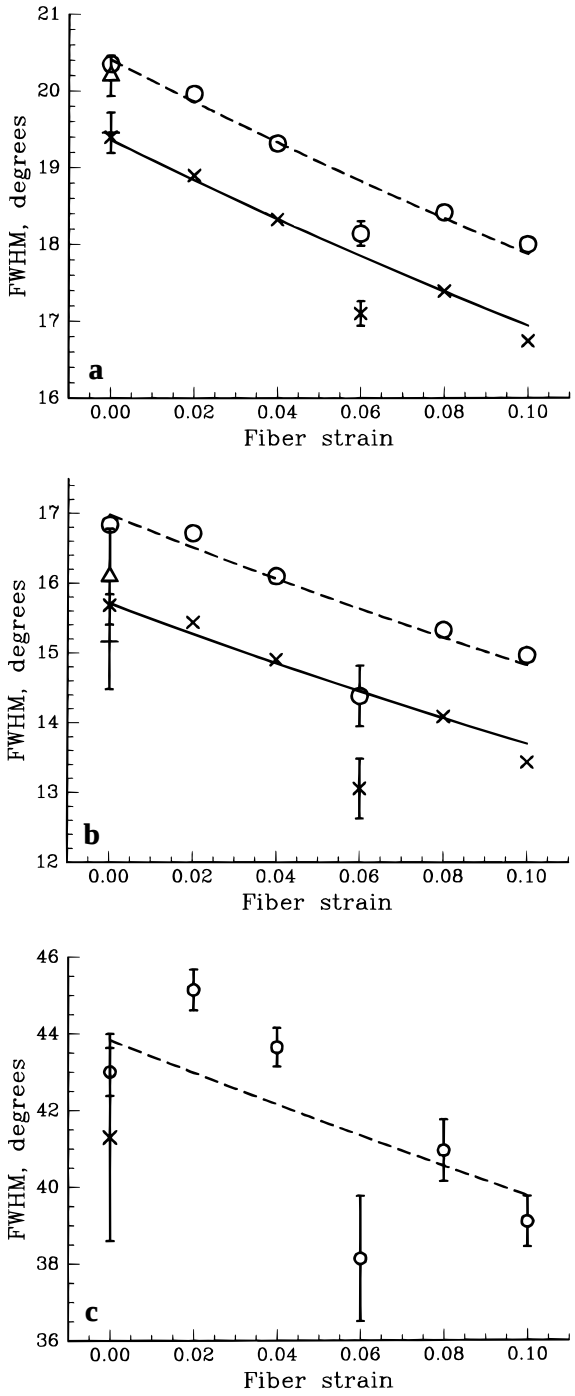

Figure 4. Chain axis orientation about the fiber axis as a function of fiber strain, as derived from the fitted equatorial intensity distributions as shown in Figure 2. In (a) and (b) the circles and the dashed line are from the angular data, and the triangles and the solid line are from angular data corrected for reflection widths. Key: (a) orientation of all anisotropic material, from the Pearson VII function fit of equatorial data; (b) orientation of crystalline material, from the narrow Gaussian part of the two-Gaussian fit of equatorial data; (c) orientation of the oriented non-crystalline material, from the broad Gaussian part of the two-Gaussian fit of equatorial data.

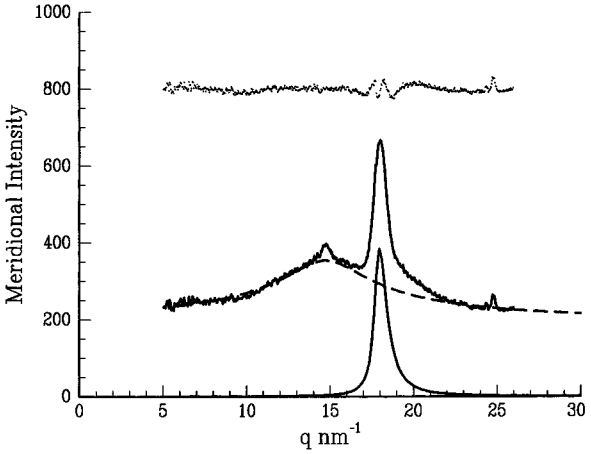

Figure 5. Intensity as a function of scattering vector $q = 4\pi(\sin\theta)/\lambda$ along the meridian. Note the strongly asymmetric shape of the (002) reflection.

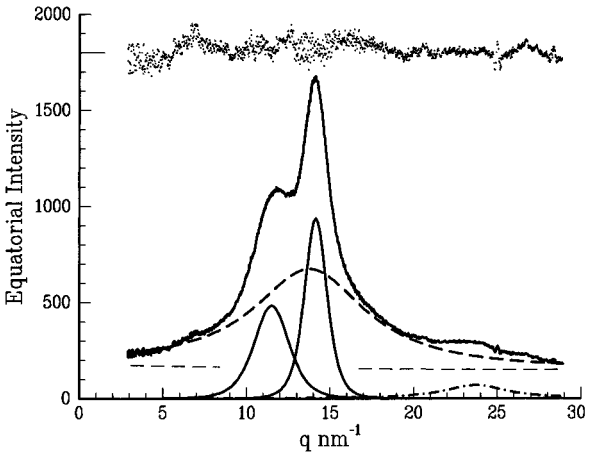

Figure 6. Intensity as a function of scattering vector $q = 4\pi(\sin\theta)/\lambda$ along the equator and its deconvolution into two crystalline peaks, an amorphous halo, and a broad peak at high diffraction angle that is caused by the superposition of several weak crystalline reflections.

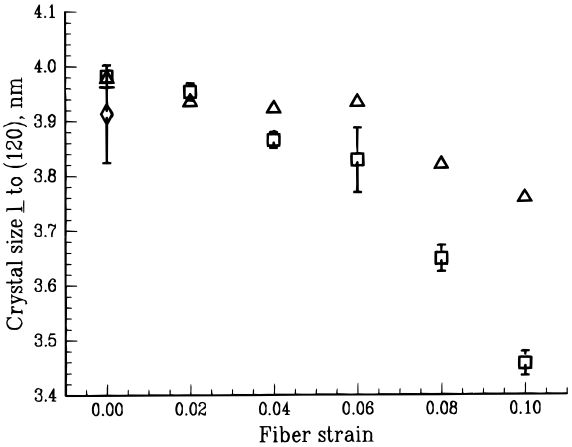

Figure 7. Effect of tensile deformation on the lateral crystal sizes, as obtained from the widths of the (120) and (200) peaks by the Scherrer equation.

improving the calculated orientation for each component. The lower data sets in parts a and b of Figure 4 are corrected in this way, using the (002) width from each pattern. The result is to reduce the fwhm by about a degree to 19.5° when all oriented material is included and to 15.7° for the crystals. The solid lines are the fit to affine deformation with one free variable, the orientation at zero strain. The greater misorientation of the oriented amorphous component means that the effect of the correction is only 0.5°, and the greater scatter makes this insignificant. The angular width of the (002) corresponds to a reflection width of 155 pixels, and the radial widths of the (120) and (200) are 35 and 62 pixels respectively. The exponent in the Pearson VII functions for the radial widths are lower, and this makes the

deconvolution have a slightly larger effect, a 10% reduction from 21 to 19° fwhm.

Crystallinity. X-ray crystallinity measurements from powdered samples of spider silk have previously been attempted[29] following procedures used for Bombyx mori silk,[2,27] where the degree of crystallinity as about 65%.[27] The attempts were not very successful. The silk from *N. clavipes* diffracted weakly, but worse than that, it was not possible to separate the overlapping broad crystalline reflections from the amorphous halo. The orientation in the fiber separates the crystal reflections and makes them all clearly distinguishable from the amorphous scattering. Despite this advantage, crystallinity cannot normally be measured from a fiber pattern. The orientation enhances some reflections and suppresses others, and the flat plate geometry does not collect data at large enough values of s. Here the smaller wavelength, 0.091 nm compared to the usual 0.154 nm, gives a somewhat larger range of s, and because the crystals are so imperfect, there are no significant detectable crystalline reflections at higher angles. If ideal fiber symmetry is assumed, it is possible to take orientation into account by correcting all the observed intensities for orientation. They can then be added to calculate a powder diffraction pattern where the contributions of crystalline and amorphous scatter are known. From this data the crystallinity X_C can be determined using the method of Ruland[30] as described in Balta-Calleja and Vonk.[31]

To obtain the crystallinity, the first step was to take radial scans at many positions, and through all visible crystalline reflections. After the equivalent scans from an exposure taken with no sample present were subtracted the peaks were fitted as Pearson VII functions. Angular scans were also taken through all the reflections. The peaks were then corrected for polarization (the synchrotron beam is horizontally polarized), for fiber geometry by multiplying by the square of the equatorial component of s, s_x^2, for multiplicity, and finally for angular spread in the detector plane by multiplying by the angular fwhm. Adding all the corrected fitting functions gives the equivalent corrected crystalline powder intensity $i_c s^2$. The equivalent corrected total powder intensity $I_T s^2$ was obtained by adding the corrected intensity of the oriented amorphous halo, the isotropic halo, and the continuous background. The oriented halo was treated in the same way as a crystalline reflection. The isotropic components were estimated from weighted averages of radial scans that missed the crystalline reflections as much as possible, and their multiplicity × angular width was set to 340 to give the correct total relative intensity for a uniform ring.

From here on the data could be treated as if it had been obtained from a powder. The "structure free" coherent, I_{coh}, and incoherent, I_{inc}, scatter were calculated from the chemical composition of the material and tabulated values of atomic form factors and incoherent scattering functions. The total matched the form of I_T at $s > 2$ nm^{-1}, although a limit of 5−6 nm^{-1} is usually preferred.[31] The scaling factor from this match, T, is used to remove the correct amount of incoherent scattering from the total intensity I_T; $i = I_T - I_{inc}/T$.

$$T = \frac{\int_0^{s_p} (I_{coh} + I_{inc}) s^2 \, ds}{\int_0^{s_p} I_T s^2 \, ds} \qquad (3)$$

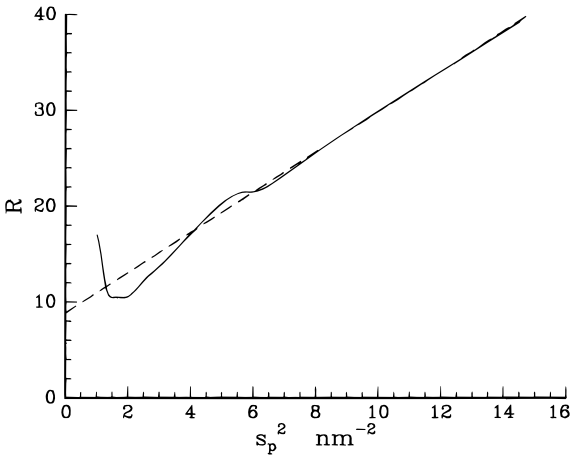

Figure 8. Plot of the ratio R vs the upper integration limit s_p. The dashed line is the linear fit in the range 8−13, with an intercept of $R(0) = 1/X_C = 8.5$.

The ratio of corrected total intensity to intensity arising from observable crystalline reflections is then calculated as

$$R = \frac{\int_0^{s_p} i s^2 \, ds}{\int_0^{s_p} i_c s^2 \, ds} \qquad (4)$$

A plot of R vs s_p^2 should be a straight line at low s_p or a parabola, and the intercept at $s_p = 0$ is $1/X_C$. Here although there is a reasonable data range where the plot is a straight line, Figure 8, the data range is too narrow. The intercept depends on the region chosen to be fitted. From the "best" choices of continuous background function and fitting region, as chosen by the human eye, the result is $X_C = 11.8\%$. With a wide range of reasonable choices, the result lies within the region of 10−15%, so the best estimate for crystallinity is 12 ± 3%. The corrected peak areas for the isotropic and oriented amorphous peaks are in the ratio 63:40. Applying this to the 88% that is noncrystalline gives 54% for the isotropic and 34% for the oriented material. Adding $\langle \cos^2 \phi_3 \rangle$ for each component gives an overall average of 0.60, with $f = 0.39$ for the whole fiber. It should be noted that the percentages given above apply to the fibers under the conditions of exposure, 23 °C, and 34% relative humidity. Any water present in the fiber will contribute to the isotropic amorphous component, increasing the true crystallinity of the dry fiber.

Because this correct determination of crystallinity is so time consuming, it was only performed once. We have also estimated the crystallinity for a range of samples by comparing the total intensity in the (120) and (200) reflections, which seem to dominate the crystalline pattern, to the intensity in the amorphous halo. Although it does not appear so from the overall pattern (Figure 1), or from the radial intensity plot in Figure 5, the total integrated intensities of the two crystalline peaks are almost equal. The (120) seems much stronger, but the peak is narrower. The crystallinity on this basis is 13 ± 3% for all dry silk samples, where the error relates only to the range of values obtained from the different samples. This is in sufficient agreement with the one detailed calculation for this measurement to be a useful comparative tool. From the full calculation it is apparent that the agreement is fortuitous. After correction, the first layer line reflections contain as much integrated intensity as the two

apparently stronger equatorials, and the other weaker visible reflections add nearly as much again. This extra crystalline intensity just happens to be offset by the large integrated intensity of the continuous background, ignored in the simple estimate.

Comparison with Previous Results. Work and Morosoff[13] used X-ray diffraction to determine the orientation distribution of crystals in fibers of spider major ampullate silk. They give values of $\langle\cos^2\phi_3\rangle$ for molecular chain orientation in the crystals of 0.776 and 0.788, with $f \approx 0.67$. This corresponds to fwhm of about 70° for a Gaussian distribution, much larger than our uncorrected result of 20.5° ($f = 0.97$). The silk did come from different species of spiders, but the diffraction patterns (Figures 6 and 7 of ref 13) are very similar to Figure 1. Values of $\langle\cos^2\varphi\rangle$ for (120) are also given in ref 13. They are close to 0.11, and this corresponds to a fwhm of 48° for Ψ, again much larger than the present result (14°, Table 1) and larger than seems possible from the figures in ref 13. If 0.11 is taken as $\cos^2[\text{fwhm}(\varphi)]$, then a more reasonable value of 19° is obtained for the fwhm of Ψ. The overall average orientation was measured for the same fibers using birefringence[32] with results of $f = 0.43$ for *Nephila cruentata* and $f = 0.65$ for *Araneus marmoreus*. The difference is much larger than the difference in crystalline orientations, it prevents useful comparisons with the current result of $f = 0.39$ for *N. clavipes*.

The NMR results for orientation were a fwhm of 5 $(-2 + 8)$° for the alanine crystals, and 75 ± 5° for the remainder of the alanine residues.[10] The deuterated methyl group is perpendicular to the chain, so the comparison to X-ray data should be made with the orientation of the equatorial reflections and not the derived chain axis orientation. These are approximately 11° and 30°, as shown in Table 1. Although the NMR results focus only on the alanine residues, and the X-ray results reflect the entire sample, the NMR-determined fwhm for the crystalline fraction is in good agreement with the present data. One possible interpretation of this agreement is that the crystalline regions are largely comprised of alanine. The second component in the X-ray data, with a fwhm of 30°, is much more highly oriented than the average orientation found by NMR for the rest of the alanines. This suggests that alanine residues make up only a small part of this component.

The crystallinity derived here, 12%, is lower than the usually quoted values of 30−50%.[2] However, these values are often of uncertain origin, deriving from analogy with *B. mori* silk, which is more crystalline than the spider dragline silk. NMR has shown that 40% of the alanine residues in spider dragline silk reside in highly oriented crystalline domains.[10,11] From the chemical composition, this is about 10% of the whole fiber. If the crystals are pure poly(alanine), this is the crystallinity and it is the same as the X-ray result, allowing for the uncertainties of measurement. However, it is easy to explain a greater value for the X-ray crystallinity, since the smaller glycine residues may be incorporated in a crystal with the poly(alanine) structure. This would increase the crystalline content beyond the alanine content. More generally, exact agreement should not be expected because the two methods are sensitive to different things. In a simple model of perfect small crystals of poly(alanine), the regions of three-dimensional spatial order and the regions where the alanines are restricted in their motion are the same. In any more complicated situation, they may be different.

Mechanical modeling of the stiffness of the fibers, either by regarding it as a filled elastomer[2,5] or using a micromechanical composite model[33] requires more than 12% crystallinity. Termonia used 50% volume fraction of crystals, and still needed a surface layer of intermediate mechanical properties around the crystals in order to model the stiffness and strength of the fiber.[33] This indicates that the "oriented amorphous" material must have mechanical properties that are much better than that of regular amorphous material.

Conclusions

A detailed analysis of X-ray fiber pattern from spider silk shows a well oriented crystalline component —orientation function 0.981—which makes up only 12% of the material. Another one third of the fiber material is oriented—orientation function 0.87—but the X-ray reflection from this component is radially so broad that it the material is amorphous by the normal standards of X-ray diffraction. The remainder is amorphous and isotropic. The crystal size obtained by applying the simple Scherrer formula to the crystalline peak widths is approximately 5 × 2 × 7 nm along **a**, **b**, and **c**. These dimensions are lower limits, in that an imperfect crystal of greater size would show similar broadening. The lateral sizes are also the averages of broad distributions.

The crystals clearly re-orient when the fiber is stretched, and the observed change is very close to the prediction of affine deformation. If the material is acting as a filled elastomer, with the crystals as rigid inclusions, then they should reorient in this way. A stretched elastomer should also increase the orientation of the amorphous material, and when it is fully relaxed the orientation should fall to zero. There was some indication of a reorientation of the amorphous material in these experiments, but the scatter was large and the strain range very limited. A larger strain range can be obtained by starting with a fiber fully relaxed by the action of water, and these experiments are in progress.

Acknowledgment. We are grateful to Isaac Trefz, for his work in setting up Matlab macros and other elements of the data analysis, and to Zhitong Yang, Steven M. Lee, Richard Do, and Joseph Wehman for collecting silk samples. The data could not have been collected without the help and guidance of CHESS and MACChess staff. Funding from National Textile Council and the National Science Foundation (Grant MCB-9601018) is gratefully acknowledged.

References and Notes

(1) Zemlin, J. C. Technical Report 69-29-CM; U.S. Army Natick Laboratories: Natick, MA, 1968.
(2) Gosline, J. M.; DeMont, M. E.; Denny, M. W. *Endeavour* **1986**, *10*, 37.
(3) Hinman, M. B.; Lewis, R. V. *J. Biol. Chem.* **1992**, *267*, 19320.
(4) Jackson, C.; O'Brien, J. P. *Macromolecules* **1995**, *28*, 5975.
(5) Prince, J. T.; McGrath, K. P.; DiGirolamo, C. M.; Kaplan, D. L. *Biochemistry* **1995**, *34*, 10879.
(6) Marsh, R. E.; Corey, R. B.; Pauling, L. *Biochim. Biophys. Acta* **1955**, *16*, 1.
(7) Warwicker, J. O. *J. Mol. Biol.* **1960**, *2*, 350.
(8) Becker, M. A.; Mahoney, D. V.; Lenhert, P. G.; Eby, R. K.; Kaplan, D.; Adams, W. W. In *Silk Polymers: Materials Science and Biotechnology*; Kaplan, D., Adams, W. W., Farmer, B., Viney, C., Eds.; ACS Symposium Series 544; American Chemical Society: Washington, DC, 1994; p 185.

(9) Marsh, R. E.; Corey, R. B.; Pauling, L. *Acta Crystallogr.* **1955**, *8*, 710.
(10) Simmons, A. H.; Ray, E.; Jelinski, L. W. *Science* **1996**, *271*, 84.
(11) Simmons, A. H.; Michal, C. A.; Jelinski, L. W. *Macromolecules* **1994**, *27*, 5235.
(12) Nakamae, K.; Nishino, T.; Ohkubo, H. *Polymer* **1989**, *30*, 1243.
(13) Work, R. W.; Morosoff, N. *Text. Res. J.* **1982**, *52*, 349.
(14) Work, R. W. *J. Exp. Biol.* **1985**, *118*, 379.
(15) Gosline, J. M.; Denny, M. W.; DeMont, M. E. *Nature* **1984**, *309*, 551.
(16) Mandelkern, L. *Chemtracts: Macromol. Chem*. **1992**, *3*, 347.
(17) Fu, Y.; Busing, W. R.; Jin, Y.; Affholter, K. A.; Wunderlich, B. *Macromol. Chem. Phys.* **1994**, *195*, 803.
(18) Havens, J. R.; VanderHart, D. L. *Macromolecules* **1985**, *18*, 1663.
(19) Thiel, B. D.; Kunkel, D. D.; Viney, C. *Biopolymers* **1994**, *34*, 1089.
(20) Thiel, B. L.; Viney, C. *MRS Bull.* **1995**, Sept, 52.
(21) Work, R. W.; Emerson, P. D. *J. Arachnol.* **1982**, *10*, 1.
(22) Ianelli, P.; Immirzi, A. *Macromolecules* **1990**, *23*, 2375.
(23) Busing, W. R. *Macromolecules* **1990**, *23*, 4608.
(24) Fu, Y.; Busing, W. R.; Jin, Y.; Affholter, K. A.; Wunderlich, B. *Macromolecules* **1993**, *26*, 2187.
(25) Arnott, S.; Dover, S. D.; Elliott, A. *J. Mol Biol.* **1967**, *30*, 201.
(26) McNamee, S. G.; Ober, C. K.; Jelinski, L. W.; Ray, E.; Xia, Y.; Grubb, D. T. In *Silk Polymers: Materials Science and Biotechnology*; Kaplan, D., Adams, W. W., Farmer, B., Viney, C., Eds.; ACS Symposium Series; American Chemical Society: Washington, DC, 1994; p 176.
(27) Nadiger, G. S.; Halliyal, V. G. *Colourage* **1984**, *31*, 23.
(28) Kaplan, D. L.; Lombardi, S. J.; Muller, W. S.; Fossey, S. A. In *Biomaterials: Novel Materials from Biological Sources*; Byrom, D., Ed.; Stockton Press: New York, 1991; p 2.
(29) Grubb, D. T. Unpublished data.
(30) Ruland, W. *Acta Crystallogr.* **1961**, *14*, 1180.
(31) Balta-Calleja, F. J.; Vonk, C. G. *X-ray Scattering of Synthetic Polymers (Polymer Science Library Vol. 8)*; Elsevier: Amsterdam, New York, 1989; Section 5.3.3.
(32) Fornes, R. E.; Work, R. W.; Morosoff, N. *J. Polym. Sci., Polym. Phys. Ed.* **1983**, *21*, 1163.
(33) Termonia, Y. *Macromolecules* **1994**, *27*, 7378.

MA961293C